Near-field Target Localization for EMVS-MIMO Radar with Arbitrary Configuration

Hua Chen, *Senior Member, IEEE*, Jiaxiong Fang, Weilong Wang, Wei Liu, *Senior Member, IEEE*, Ye Tian, *Member, IEEE*, Qing Wang, *Member, IEEE* and Gang Wang, *Senior Member, IEEE*

***Abstract*—A three-dimensional (3-D) near-field (NF) source localization method is introduced for a bistatic multiple-input multiple-output (MIMO) radar system equipped with arbitrary electromagnetic vector sensors (EMVSs) at both the transmitter and receiver. Firstly, to obtain estimates of the steering matrices of the transmitting array and the receiving array, tensor decomposition is performed on the covariance matrix of the outputs. Then, multiple parameters of targets, including two-dimensional direction-of-departure (2D-DOD), range from transmitter to target (RFTT), along with two-dimensional direction-of-arrival (2D-DOA), range from target to receiver (RFTR), and two-dimensional receive polarization angle (2D-RPA) with respect to receiver can be obtained by exploiting the property of rotation invariance. Subsequently, a linear equation can be constructed to determine all location parameters of NF targets. The proposed method can provide automatically paired multi-parameters without peak search and has low computational complexity. Moreover, the Cramer-Rao bound (CRB) is derived as a performance benchmark for the model under consideration, and the effectiveness of the proposed method is illustrated by a series of numerical simulations.**

***Index Terms*—near-field, multiple-input multiple-output, electromagnetic vector sensors, tensor decomposition.**

I. Introduction

Multiple-input multiple-output (MIMO) radar has garnered lots of interest in the realm of array signal processing over the last few decades [1–7]. Utilizing waveform and spatial diversity techniques, MIMO radar demonstrates superior performance over the conventional phased array radar in terms of identifiability, resolution and anti-interference capability [8].

Since bistatic MIMO radar is a special case of MIMO radar, various parameter estimation algorithms, including those based on multiple signal classification (MUSIC) [9], estimation of signal parameters via rational invariance techniques (ESPRIT) [10] and tensor decomposition [11], have been developed. The methods in [9–11] are based on linear scalar sensor arrays, primarily focused on one-dimensional (1-D) direction-of-departure (DOD) and direction-of-arrival (DOA) estimation, while in [12, 13], several methods are proposed with the aim of obtaining two-dimensional (2D)-DOD and 2D-DOA estimations. However, these methods are all developed based on scalar sensor arrays only measuring the spatial information, incapable of perceiving the polarization information of electromagnetic signals, which is of great significance in practice [14]. In contrast to scalar sensors, an electromagnetic vector sensor (EMVS) is composed of three orthogonally polarized electric dipoles and three orthogonal magnetic loops [15], which can not only achieve 2-D direction finding, but also measure the auxiliary polarization angles and polarization phase differences. For this purpose, electromagnetic vector sensors are employed in bistatic MIMO radar to jointly estimate 2D angle and polarization parameters of the targets[16].

As an emerging radar system, polarized MIMO radar can measure both the spatial and polarization domain information of the targets. A series of studies have been performed to realize parameter estimation for such kind of MIMO radar. With the use of the rotational invariance property, a method is presented in [17] to acquire 2D estimates for a bistatic MIMO radar system equipped with a uniform linear array (ULA) comprising several EMVSs in both its transmitter and receiver, which requires further pairing operations. To address the limitations in [17], a parallel factor (PARAFAC) estimator is developed in [18], which can obtain automatically paired multiple parameters of interest. However, the methods in [17, 18] are only adequate for ULA with half-wavelength spacing. To this end, an L-shaped sparse array geometry for a bistatic EMVS-MIMO radar is introduced in [19], which is applicable to linear arrays whose inter-element spacing exceeds half-wavelength, and it can achieve unambiguous estimation of 2D-DOD, 2D-DOA and polarization parameters with high resolution. An improved subspace method exploiting the relationship of rotational invariance and the normalized Poynting-vectors is presented in [20] to achieve the 2D angle and polarization parameters based on a bistatic EMVS-MIMO radar system with random array geometry.

It's worth mentioning that all of the methods discussed above are dedicated to the far-field sources whose the wavefront's curvature is approximately planar. However, in practical applications, the target may be nearer to both the transmit and

This work was supported by the Zhejiang Provincial Natural Science Foundation of China under Grant LY23F010003 and LR20F010001, by the National Natural Science Foundation of China under Grants 62001256, U20A20162 and 62222109, and the UK Engineering and Physical Sciences Research Council (EPSRC) under grant EP/V009419/2, and the Key Research and Development Program of Tibet Autonomous Region, and the Science and Technology Major Project of Tibetan Autonomous Region of China under grant XZ202201ZD0006G03. For the purpose of open access, the author(s) has applied a Creative Commons Attribution (CC BY) license to any Accepted Manuscript version arising. (*Corresponding authors: Hua Chen, Ye Tian.*)

Hua Chen, Jiaxiong Fang, Weilong Wang, Ye Tian and Gang Wang are with the Faculty of Electrical Engineering and Computer Science, Ningbo University, Ningbo 315211, China. (e-mail: dkchenhua0714@hotmail.com; tianfield@126.com; wanggang@nbu.edu.cn)

Hua Chen is also with the Zhejiang Key Laboratory of Mobile Network Application Technology, Ningbo 315211, P. R. China.

Wei Liu is with the School of Electronic Engineering and Computer Science, Queen Mary University of London, London E1 4NS, UK. (e-mail: wliu.eee@gmail.com)

Qing Wang is School of Electronic Informatin Engineering, Tianjin University, Tianjin, China. (e-mail: wangq@tju.edu.cn)

receive arrays. There are currently few researches focusing on near-field (NF) parameter estimation for MIMO radar. In [21], a 4-D NF parameter estimation method based on bistatic MIMO radar is proposed, appropriate for the centro-symmetric array structure. Besides, in [22], a method is presented for jointy estimating DOA and range in a monostatic MIMO radar system. Methods based on an approximated model with Fresnel hypothesis are proposed in [21] and [22]. Although the approximated model can reduce complexity, it inevitably introduces a systematic error, resulting in decreased estimation accuracy. To improve the performance, NF source localization methods based on an accurate model are proposed in [23] and [24] for bistatic MIMO radar systems. Based on an exact spatial propagation model, both conditional and unconditional Cramer-Rao bounds (CRBs) are analyzed in [25].

The methods in [21–24] are all based on scalar arrays. As far as we know, there hasn't been much emphasis on 2-D (except for our previous research on incomplete EMVS [26]) or 3D near-field source localization in bistatic MIMO radar furnished with EMVS arrays. In this paper, a method for multi-parameter estimation, including 2D-DOD, and range from transmitter to target (RFTT), along with 2D-DOA, range from target to receiver (RFTR), and two-dimensional receive polarization angle (2D-RPA), is proposed for three-dimensional (3-D) NF sources based on bistatic MIMO radar furnished with arbitrary EMVSs at both the transmitter and receiver. The following are the principal contributions of this study.

(1) Different from the bistatic MIMO radar based on scalar arrays for near-field source localization established in [21–24], a new bistatic polarimetric MIMO radar model equipped with multiple complete EMVS at both the transmitter and receiver is established for 3D near-field source localization, and the model considers probing polarization and scattered echo polarization.

(2) The proposed method requires no paring procedure for multiple parameters and has a closed-form expression without ambiguities, which is applicable to arbitrary EMVS array geometries for 3-D NF target localization; as a benchmark for performance evaluation, the CRB for the considered model is derived.

Notations: $(\cdot)^{-1}$, $(\cdot)^{+}$, $(\cdot)^{T}$ and $(\cdot)^{H}$ signify inverse, pseudo-inverse, transpose, and conjugate transpose, respectively; $\circ$, $\odot$, $\otimes$ and $\oplus$ stand for the vector outer product, Khatri-Rao product, Kronecker product and Hadamard product, respectively; $\mathbf{I}_p$ is the $p \times p$ identity matrix, while $\mathbf{1}_p$ is the all-one $p \times 1$ column vector; $\mathbf{e}_m$ and $\mathbf{e}_n$ denote $1 \times M$ and $1 \times N$ row vectors with the mth entry and nth entry being 1 and 0 elsewhere, respectively; $\|\cdot\|_F$ represents the Frobenius norm. Re$\{\cdot\}$, angle$\{\cdot\}$, *diag*$\{\cdot\}$ and blkdiag$\{\cdot\}$ repersent diagonalization, real part, and block diagonalization operation, respectively.

II. Tensor and Parafac Decomposition Preliminaries

Tensors are high-dimensional structures with dimensions greater than or equal to three. Among them, vectors and matrices can be regarded as special cases of tensors. Typically, tensors of higher than second-order are termed higher-order tensors. The following definitions are provided to help understanding some basics of tensor and PARAFAC decomposition [27, 28].

Definition 1 (Tensor Unfolding): The mode-n matrix unfolding of a tensor is to recombine the elements of a higher-order tensor according to certain rules, and then form a matrix. That is, the mode-n matrix unfolding of the tensor $\boldsymbol{\mathcal{X}}$ can be denoted as $[\boldsymbol{\mathcal{X}}]_n$, and the $(i_1, i_2, \cdots, i_N)$-element of $\boldsymbol{\mathcal{X}}$ is mapped to the (i_n, j)-th element of $[\boldsymbol{\mathcal{X}}]_n$, where $j = 1 + \sum_{k=1, k\neq n}^{N} (i_k - 1) J_k$, $J_k = \prod_{m=1, m\neq n}^{k-1} I_m$.

Definition 2 (PARAFAC Decomposition): Tensor can be represented by the sum of a set of rank-one tensors, and the PARAFAC decomposition of a rank-K tensor $\boldsymbol{\mathcal{X}}$ can be mathematically formulated as follows

$$\boldsymbol{\mathcal{X}} = \sum_{r=1}^{K} \mathbf{v}_{1,k} \circ \mathbf{v}_{2,k} \circ \cdots \circ \mathbf{v}_{N,k}, \tag{1}$$

where $\mathbf{v}_{N,k} \in \mathbb{C}^{I_n \times 1}$. The representation of (1) in mode-n matrix unfolding format is as follows

$$[\boldsymbol{\mathcal{X}}]_n = \mathbf{V}_n [\mathbf{V}_{n+1} \odot \cdots \mathbf{V}_N \odot \mathbf{V}_1 \odot \cdots \mathbf{V}_{n-1}]^T, \tag{2}$$

where $\mathbf{V}_n = [\mathbf{v}_{n,1}, \mathbf{v}_{n,2}, \cdots, \mathbf{v}_{n,K}]$.

Definition 3 (Generalized Tensorization of a PARAFAC model): For the PARAFAC decomposition model of Eq. (1), let the order sets $\mathbb{Q}_i = \{\mathbb{Q}_{i,1}, \mathbb{Q}_{i,2}, \cdots, \mathbb{Q}_{i,M_i}\}$ for $i = 1, 2, \cdots, I$ represent a division of the dimensions $\mathbb{Q} = \{1, 2, \cdots, N\}$, and the generalized tensorization of $\boldsymbol{\mathcal{X}}$ can be represented by a new tensor $\boldsymbol{\mathcal{X}}_{\mathbb{Q}_1, \mathbb{Q}_2, \cdots, \mathbb{Q}_I} \in \mathbb{C}^{T_1 \times T_2 \times \cdots \times T_I}$ with

$$\boldsymbol{\mathcal{X}}_{\mathbb{Q}_1, \mathbb{Q}_2, \cdots, \mathbb{Q}_I} = \sum_{k=1}^{K} \mathbf{e}_k^{(1)} \circ \mathbf{e}_k^{(2)} \circ \cdots \circ \mathbf{e}_k^{(I)}, \tag{3}$$

where $T_i = \prod_{m=1}^{M_i} I_{\mathbb{Q}_{i,m}}$, $\mathbf{e}_k^{(i)} = \mathbf{v}_k^{(\mathbb{Q}_i, M_i)} \otimes \mathbf{v}_k^{(\mathbb{Q}_i, M_{i-1})} \otimes \cdots \otimes \mathbf{v}_k^{(\mathbb{Q}_i, 1)}$.

III. Signal Model

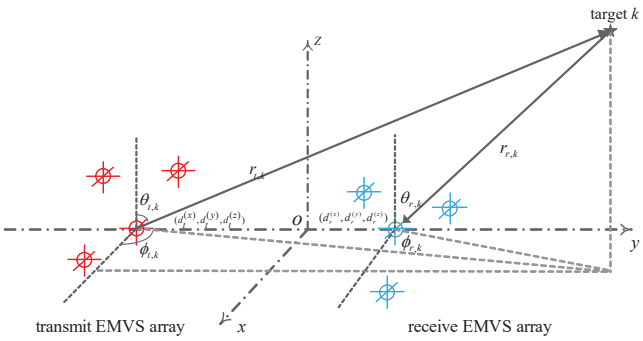

Fig. 1. Geometry of the considered bistatic EMVS-MIMO radar.

As depicted in Fig. 1, consider a bistatic MIMO radar system equipped with P and Q EMVSs at the transmitter and the receiver, respectively, where all transmit EMVSs and receive EMVSs are distributed in the 3-D space. In

addition, the position of the pth transmit EMVS and that of the qth receive EMVS can be expressed as $(x_{t,p}, y_{t,p}, z_{t,p})$ and $(x_{r,q}, y_{r,q}, z_{r,q})$, respectively. The array elements at $(d_t^{(x)}, d_t^{(y)}, d_t^{(z)})$ and $(d_r^{(x)}, d_r^{(y)}, d_r^{(z)})$ are taken as the reference elements of the transmit array and the receive array, respectively. Without loss of generality, assume that there are K uncorrelated narrow-band NF targets, and the location of the kth target is parameterized by $(\theta_{t,k}, \varphi_{t,k}, \theta_{r,k}, \varphi_{r,k}, r_{t,k}, r_{r,k})$ in which $\theta_{t,k}$ and $\varphi_{t,k}$ represent the elevation and azimuth angles of the kth target related to the transmitter, $\theta_{r,k}$ and $\varphi_{r,k}$ denote the elevation and azimuth angles of the kth target related to the receiver, $r_{t,k}$ and $r_{r,k}$ represent the range from the transmitter to the kth target and the range from the kth target to the receiver. According to Fig. 1, the range from the mth transmit EMVS to the kth target and the range from the kth target to the nth receive EMVS can be expressed as Eq. (4) and Eq. (5) at the bottom of this page. The narrowband normalized electric field signal transmitted by the pth transmit EMVS to the kth target can be expressed as [16, 29, 30].

$$\begin{aligned}&\mathbf{r}_{p,k}(t) = \mathbf{V}_{t,p,k}^T \mathbf{b}_p s_p(t)\\ &=\boldsymbol{\zeta}_{p,k} s_p(t)\\ &=\begin{bmatrix}\zeta_{p,k,H}\\ \zeta_{p,k,V}\end{bmatrix} s_p(t)\end{aligned} \tag{6}$$

where t represents the fast time index, and $\mathbf{V}_{t,p,k}$ denotes the direction matrix of the pth transmit EMVS relative to the kth target, defined as

$$\mathbf{V}_{t,p,k} = \begin{bmatrix}\cos\phi_{t,p,k}\cos\theta_{t,p,k} & -\sin\phi_{t,m,t,p,kk}\\ \sin\phi_{t,p,k}\cos\theta_{t,p,k} & \cos\phi_{t,p,k}\\ -\sin\theta_{t,p,k} & 0\\ -\sin\phi_{t,p,k} & -\cos\phi_{t,p,k}\cos\theta_{t,p,k}\\ \cos\phi_{t,p,k} & -\sin\phi_{t,p,k}\cos\theta_{t,p,k}\\ 0 & \sin\theta_{t,p,k}\end{bmatrix} \tag{7}$$

and $\mathbf{b}_p$ is the 6×1 weight vector that controls the transmit polarization waveform [31], $s_p(t)$ indicates the waveform emitted by the pth transmit EMVS. In addition, $\boldsymbol{\zeta}_{p,k}$ represents the probing polarization corresponding to the pth transmit EMVS, $\zeta_{p,k,H}$ and $\zeta_{p,k,V}$ are the horizontal and vertical components of the waveform, respectively. Assume that the transmitting array emits P mutual orthogonal waveforms $\{s_p(t)\}_{p=1}^P$, which satisfy

$$\int_{T_m} s_i(t) s_j^*(t)\, dt = \begin{cases}1, i{=}j\\ 0, \text{otherwise}\end{cases} \tag{8}$$

where T_m is the pulse duration. Then, in the line-of-sight scenario, the echo reflected by the kth target can be denoted as

$$\mathbf{r}_k(t,\tau) = u_k(\tau)\, \boldsymbol{\zeta}_{p,k}^T \mathbf{h}_{t,k}^T \mathbf{s}(t) \tag{9}$$

where τ is the pulse index, $u_k(\tau)$ denotes the reflection coefficients of the kth target, $\mathbf{s}(t) = [s_1(t), \cdots, s_P(t)]$ represents the waveform vector, $\mathbf{h}_{t,k}$ is the steering vector of the transmitting array, given by $\mathbf{h}_{t,k} = \left[c_{t,1,k} e^{j\tau_{t,1,k}}, \cdots, c_{t,P,k} e^{j\tau_{t,P,k}}\right]^T$ with $c_{t,p,k} = \frac{r_{t,k}}{r_{t,p,k}}$ being the spatial magnitude attenuation, and $\tau_{t,p,k} = \frac{2\pi}{\lambda}(r_{t,k} - r_{t,p,k})$ the spatial phase factor due to propagation delay.

Consequently, when the echo of the target is simultaneously received by the receive EMVS array, the noise-contaminated signal from the receiving EMVS array can be denotes as

$$\mathbf{x}(t,\tau) = \sum_{k=1}^{K} \mathbf{h}_{r,k} u_k(\tau)\, \mathbf{h}_{t,k}^T \mathbf{s}(t) + \mathbf{w}(t,\tau) \tag{10}$$

where $\mathbf{h}_{r,k}$ is the steering vector of the receive array, given by $\mathbf{h}_{r,k} = \left[\left[c_{r,1,k} e^{j\tau_{r,1,k}} \mathbf{a}_{r,1,k}\right]^T, \cdots, \left[c_{r,Q,k} e^{j\tau_{r,Q,k}} \mathbf{a}_{r,Q,k}\right]^T\right]^T$, and $\mathbf{a}_{r,q,k}$ represents the polarization response of the qth receive EMVS with respect to the kth target, expressed as

$$\begin{aligned}&\mathbf{a}_{r,q,k} = [\mathbf{e}_{r,q,k}, \mathbf{h}_{r,q,k}]^T\\ &= [e_{r,q,k}^{(x)}, e_{r,q,k}^{(y)}, e_{r,q,k}^{(z)}, h_{r,q,k}^{(x)}, h_{r,q,k}^{(y)}, h_{r,q,k}^{(z)}]^T\\ &=\mathbf{V}_{r,q,k}\mathbf{g}_{r,q,k}\end{aligned} \tag{11}$$

where $\mathbf{e}_{r,q,k} = \left[e_{r,q,k}^{(x)}, e_{r,q,k}^{(y)}, e_{r,q,k}^{(z)}\right]$ stands for the electric-field vector of the qth receiving EMVS relative to the kth target, $\mathbf{h}_{r,q,k} = \left[h_{r,q,k}^{(x)}, h_{r,q,k}^{(y)}, h_{r,q,k}^{(z)}\right]$ represents the magnetic-field vector of the qth receiving EMVS relative to the kth target, and $\mathbf{V}_{r,q,k}$ indicates the direction matrix of the qth receiving EMVS relative to the kth target, which can be denoted as

$$\mathbf{V}_{r,q,k} = \begin{bmatrix}\cos\phi_{r,q,k}\cos\theta_{r,q,k} & -\sin\phi_{r,q,k}\\ \sin\phi_{r,q,k}\cos\theta_{r,q,k} & \cos\phi_{r,q,k}\\ -\sin\theta_{r,q,k} & 0\\ -\sin\phi_{r,q,k} & -\cos\phi_{r,q,k}\cos\theta_{r,q,k}\\ \cos\phi_{r,q,k} & -\sin\phi_{r,q,k}\cos\theta_{r,q,k}\\ 0 & \sin\theta_{r,q,k}\end{bmatrix} \tag{12}$$

and $\mathbf{g}_{r,q,k}$ denotes the polarization vector that is only related to $\gamma_{r,q,k}$ and $\eta_{r,q,k}$ with $\boldsymbol{\Xi}_{p,k} \in \mathbb{C}^{2\times 2}$ being the polarization scattering matrix corresponding to the pth transmit waveform,

$$r_{t,p,k} = \sqrt{\left(r_{t,k}u_{t,k} + d_t^{(x)} - x_{t,p}\right)^2 + \left(r_{t,k}v_{t,k} + d_t^{(y)} - y_{t,p}\right)^2 + \left(r_{t,k}w_{t,k} + d_t^{(z)} - z_{t,p}\right)^2} \tag{4}$$

$$r_{r,q,k} = \sqrt{\left(r_{r,k}u_{r,k} + d_r^{(x)} - x_{r,q}\right)^2 + \left(r_{r,k}v_{r,k} + d_r^{(y)} - y_{r,q}\right)^2 + \left(r_{r,k}w_{r,k} + d_r^{(z)} - z_{r,q}\right)^2} \tag{5}$$

where $u_{t,k} = \sin\theta_{t,k}\cos\phi_{t,k}$, $v_{t,k} = \sin\theta_{t,k}\sin\phi_{t,k}$, $w_{t,k} = \cos\theta_{t,k}$, $u_{r,k} = \sin\theta_{r,k}\cos\phi_{r,k}$, $v_{r,k} = \sin\theta_{r,k}\sin\phi_{r,k}$, and $w_{r,k} = \cos\theta_{r,k}$.

describing the polarization transform property of the kth target relative to the pth transmit EMVS [32], expressed as

$$\mathbf{g}_{r,q,k} = \mathbf{\Xi}_{p,k}\boldsymbol{\zeta}_{p,k} = \begin{bmatrix} \sin\gamma_{r,q,k}e^{j\eta_{r,q,k}} \\ \cos\gamma_{r,q,k} \end{bmatrix} \tag{13}$$

with $\gamma_{r,q,k}$ and $\eta_{r,q,k}$ represent the polarization auxiliary angle and polarization phase difference of the qth receive EMVS relative to the kth target.

Thereafter, in the presence of a non-dispersive propagation environment [11], matched filtering $\mathbf{x}(t,\tau)$ by resorting to $s_p(t)$ yields

$$\begin{aligned} \mathbf{y}_p(\tau) &= \textstyle\int_{T_m} \mathbf{x}(t,\tau)s_p^*(t)\,dt \\ &= \sum_{k=1}^{K} u_k(\tau)\,\mathbf{h}_{t,k}(p)\,\mathbf{h}_{r,k} + \mathbf{n}_p(\tau) \end{aligned} \tag{14}$$

where $\mathbf{n}_p(\tau) = \int_{T_m} \mathbf{w}(t,\tau)s_p^*(t)\,dt$.

By stacking all the matched filter outputs column by column, we have

$$\begin{aligned} \mathbf{y}(\tau) &= \sum_{k=1}^{K} [\mathbf{h}_{t,k} \otimes \mathbf{h}_{r,k}]u_k(\tau) + \mathbf{n}(\tau) \\ &= (\mathbf{H}_t \odot \mathbf{H}_r)\,\mathbf{u}(\tau) + \mathbf{n}(\tau) \end{aligned} \tag{15}$$

where $\mathbf{H}_t = [\mathbf{h}_{t,1}, \mathbf{h}_{t,2}, \cdots, \mathbf{h}_{t,K}]$ and $\mathbf{H}_r = [\mathbf{h}_{r,1}, \mathbf{h}_{r,2}, \cdots, \mathbf{h}_{r,K}]$ represent the array manifold matrices of the transmitting and receiving arrays, respectively, $\mathbf{u}(\tau) = [u_1(\tau), \cdots, u_K(\tau)]^T$, $\mathbf{n}(\tau) = \left[\mathbf{n}_1^T(\tau), \cdots, \mathbf{n}_P^T(\tau)\right]^T$.

IV. The Proposed Algorithm

A. PARAFAC Decomposition

With the assumption that the NF targets are uncorrelated, the covariance matrix of $\mathbf{y}(t)$ can be expressed as

$$\begin{aligned} \mathbf{R} &= E[\mathbf{y}(\tau)\,\mathbf{y}^H(\tau)] \\ &= [\mathbf{H}_t \odot \mathbf{H}_r]\mathbf{R}_u[\mathbf{H}_t \odot \mathbf{H}_r]^H + \sigma_n^2\mathbf{I}_{6PQ} \end{aligned} \tag{16}$$

where $\mathbf{R}_s = \mathrm{E}[\mathbf{u}(t)\mathbf{u}^{\mathrm{H}}(t)] = \mathrm{diag}([\sigma_1^2, \sigma_2^2, \cdots, \sigma_K^2])$ with $k = 1, 2, \cdots, K$ being the corresponding signal power.

With a finite number L of snapshots, $\mathbf{R}$ can be estimated through

$$\hat{\mathbf{R}} = \frac{1}{L}\sum_{\tau=1}^{L}\mathbf{y}(\tau)\mathbf{y}^H(\tau) \tag{17}$$

Based on [27], $\mathbf{R}$ can be structured into a fourth-order tensor as follows

$$\boldsymbol{\mathcal{R}} = \boldsymbol{\mathcal{R}}_{s\times 1}\mathbf{H}_{t\times 2}\mathbf{H}_{r\times 3}\mathbf{H}_{t\times 4}^*\mathbf{H}_r^* + \sigma_k^2\boldsymbol{\mathcal{I}} \tag{18}$$

where $\boldsymbol{\mathcal{R}}_{s\times 1}$ denotes a diagonal tensor with its (i,i,i,i)th $(i = 1, \cdots, 4)$ entry being σ_k^2 and zeros elsewhere, and $\boldsymbol{\mathcal{I}}$ represents the tensor form of $\mathbf{I}_{6PQ}$.

Estimates of $\mathbf{H}_t$ and $\mathbf{H}_r$ can be obtained through the following formulation

$$\min_{\mathbf{H}_t,\mathbf{H}_r,\mathbf{R}_s} \|\,\hat{\boldsymbol{\mathcal{R}}} - \boldsymbol{\mathcal{R}}_{s\times 1}\mathbf{H}_{t\times 2}\mathbf{H}_{r\times 3}\mathbf{H}_{t\times 4}^*\mathbf{H}_r^*\|_F \tag{19}$$

by directly applying the quadrilinear alternating least squares (QALS) technique [33]. Nevertheless, QALS is susceptible to initial conditions and often experiences a slow convergence speed. Therefore, in this paper, the complex parallel factor analysis (COMFAC) algorithm, which is a fast and robust version of the alternating least squares method, can be adopted to accelerate its convergence. Furthermore, in order to reduce computational complexity, $\boldsymbol{\mathcal{R}}$ is required to be compressed into a third-order tensor. In accordance with Definition 2, let $\mathbb{Q}_1 = \{1\}, \mathbb{Q}_2 = \{2\}$, and $\mathbb{Q}_3 = \{3,4\}$, and then Eq. (18) can be rewritten as follows

$$\tilde{\boldsymbol{\mathcal{R}}} = \boldsymbol{\mathcal{F}}_{3,K\times 1}\mathbf{H}_{r\times 2}\mathbf{H}_{t\times 3}\tilde{\mathbf{H}}^* + \sigma_k^2\tilde{\boldsymbol{\mathcal{I}}} \tag{20}$$

where $\boldsymbol{\mathcal{F}}_{3,K\times 1}$ denotes a $K\times K\times K$ identity tensor, $\tilde{\boldsymbol{\mathcal{I}}}$ denotes the related tensor form, and $\tilde{\mathbf{H}}^* = \mathbf{H}_{r\times 4}^*\mathbf{H}_t^*$.

With Definition 3, $\tilde{\mathcal{R}}$ can be transformed into a matrix format as

$$[\tilde{\boldsymbol{\mathcal{R}}}]_{(1)}^T = (\tilde{\mathbf{H}}^* \odot \mathbf{H}_r)\mathbf{H}_t^T \tag{21}$$

$$[\tilde{\boldsymbol{\mathcal{R}}}]_{(2)}^T = (\mathbf{H}_t \odot \tilde{\mathbf{H}}^*)\mathbf{H}_r^T \tag{22}$$

$$[\tilde{\boldsymbol{\mathcal{R}}}]_{(3)}^T = (\mathbf{H}_t \odot \mathbf{H}_r)(\tilde{\mathbf{H}}^*)^T \tag{23}$$

Then, based on Eqs. (16-18), the factor matrices $\mathbf{H}_t$, $\mathbf{H}_r$ and $\tilde{\mathbf{H}}^*$ can be estimated through the following fitting

$$\min_{\mathbf{H}_t,\mathbf{H}_r,\tilde{\mathbf{H}}^*} \|\,[\tilde{\boldsymbol{\mathcal{R}}}]_{(1)}^T - (\tilde{\mathbf{H}}^* \odot \mathbf{H}_r)\mathbf{H}_t^T\|_F \tag{24}$$

$$\min_{\mathbf{H}_t,\mathbf{H}_r,\tilde{\mathbf{H}}^*} \|\,[\tilde{\boldsymbol{\mathcal{R}}}]_{(2)}^T - (\mathbf{H}_t \odot \tilde{\mathbf{H}}^*)\mathbf{H}_r^T\|_F \tag{25}$$

$$\min_{\mathbf{H}_t,\mathbf{H}_r,\tilde{\mathbf{H}}^*} \|\,[\tilde{\boldsymbol{\mathcal{R}}}]_{(3)}^T - (\mathbf{H}_t \odot \mathbf{H}_r)(\tilde{\mathbf{H}}^*)^T\|_F \tag{26}$$

Subsequently, let $\hat{\mathbf{H}}_t$, $\hat{\mathbf{H}}_r$ and $\hat{\tilde{\mathbf{H}}}^*$ denote the estimates of $\mathbf{H}_t$, $\mathbf{H}_r$ and $\tilde{\mathbf{H}}^*$, respectively. $\hat{\mathbf{H}}_t$, $\hat{\mathbf{H}}_r$ and $\hat{\tilde{\mathbf{H}}}^*$ can be calculated via

$$\hat{\mathbf{H}}_t^T = (\tilde{\mathbf{H}}^* \odot \mathbf{H}_r)^+[\tilde{\boldsymbol{\mathcal{R}}}]_{(1)}^T \tag{27}$$

$$\hat{\mathbf{H}}_r^T = (\mathbf{H}_t \odot \tilde{\mathbf{H}}^*)[\tilde{\boldsymbol{\mathcal{R}}}]_{(2)}^T \tag{28}$$

$$(\hat{\tilde{\mathbf{H}}}^*)^T = (\mathbf{H}_t \odot \mathbf{H}_r)[\tilde{\boldsymbol{\mathcal{R}}}]_{(3)}^T \tag{29}$$

Finally, the estimates of $\mathbf{H}_t$, $\mathbf{H}_r$ and $\tilde{\mathbf{H}}^*$ can be obtained by the trilinear alternating least squares (TALS) method [13]. Much like QALS, TALS exhibits a very poor convergence performance. Therefore, the COMFAC algorithm is used to generate the estimates of $\mathbf{H}_t$, $\mathbf{H}_r$ and $\tilde{\mathbf{H}}^*$ in this paper.

Remark: In order to ensure the uniqueness of PARAFAC decomposition, according to the Kruskal's theorem [11], the ranks of $\mathbf{H}_t$, $\mathbf{H}_r$ and $\tilde{\mathbf{H}}^*$ must satisfy

$$k_{\mathbf{H}_t} + k_{\mathbf{H}_r} + k_{\tilde{\mathbf{H}}^*} \geq 2K + 3. \tag{30}$$

B. Parameter Estimation

Following the normalization of $\hat{\mathbf{H}}_t$, the estimate $\hat{c}_{t,p,k}$ of the spatial amplitude attenuation of the pth transmit array element relative to the kth target can be extracted from the estimate $\hat{\mathbf{H}}_t$ of the transmit array steering matrix. Consequently, we have $\hat{c}_{t,p,k} = \mathrm{abs}\left(\hat{\mathbf{H}}_t(p,k)\right)$.

Then, based on Eq. (4), we can construct a system of linear equations for $\hat{r}_{t,k}$, $\hat{\theta}_{t,k}$ and $\hat{\phi}_{t,k}$, which can be denoted as

$$\begin{aligned}\underbrace{\begin{bmatrix} \frac{1}{\hat{c}_{t,1,k}}-1 & \cdots & \frac{1}{\hat{c}_{t,P,k}}-1 \\ -2X_{t,1} & \cdots & -2X_{t,P} \\ -2Y_{t,1} & \cdots & -2Y_{t,P} \\ -2Z_{t,1} & \cdots & -2Z_{t,P} \end{bmatrix}^T}_{\mathbf{F}_{t,k}} \underbrace{\begin{bmatrix} \hat{r}_{t,k}^2 \\ r_{t,k}u_{t,k} \\ r_{t,k}v_{t,k} \\ r_{t,k}w_{t,k} \end{bmatrix}}_{\mathbf{\Theta}_{t,k}} \\ = \underbrace{\begin{bmatrix} X_{t,1}^2+Y_{t,1}^2+Z_{t,1}^2 \\ \vdots \\ X_{t,P}^2+Y_{t,P}^2+Z_{t,P}^2 \end{bmatrix}}_{\mathbf{G}_{t,k}}\end{aligned} \tag{31}$$

where $X_{t,p} = d_t^{(x)} - x_{t,p}$, $Y_{t,p} = d_t^{(y)} - y_{t,p}$ and $Z_{t,p} = d_t^{(z)} - z_{t,p}$.

Furthermore, $\mathbf{\Theta}_{t,k}$ can be calculated via

$$\hat{\mathbf{\Theta}}_{t,k} = \left(\mathbf{F}_{t,k}^H \mathbf{F}_{t,k}\right)^{-1} \mathbf{F}_{t,k}^H \mathbf{G}_{t,k} \tag{32}$$

Therefore, 2D-DOD and RFTT can be estimated via

$$\begin{cases} \hat{\theta}_{t,k} = \arctan\left(\frac{\sqrt{\hat{\mathbf{\Theta}}_{t,k}^2(2,1)+\hat{\mathbf{\Theta}}_{t,k}^2(3,1)}}{\hat{\mathbf{\Theta}}_{t,k}(4,1)}\right) \\ \hat{\phi}_{t,k} = \arctan\left(\frac{\hat{\mathbf{\Theta}}_{t,k}(3,1)}{\hat{\mathbf{\Theta}}_{t,k}(2,1)}\right) \\ \hat{r}_{t,k} = \sqrt{\hat{\mathbf{\Theta}}_{t,k}^2(2,1) + \hat{\mathbf{\Theta}}_{t,k}^2(3,1) + \hat{\mathbf{\Theta}}_{t,k}^2(4,1)} \end{cases} \tag{33}$$

To proceed, following the normalization of $\hat{\mathbf{H}}_r$, a selection matrix, denoted by $\mathbf{J}_{r,q} = \mathbf{e}_q \otimes \mathbf{I}_6$, is defined. Accordingly, we have $\mathbf{W}_{r,q} = \mathbf{J}_{r,q}\hat{\mathbf{H}}_r$. On this basis, it is not difficult to obtain the following relationship

$$\mathrm{diag}\{\mathbf{W}_{r,q}(i,:)\} = \mathrm{diag}\{\mathbf{W}_{r,q}(j,:)\}\mathbf{\Phi}_{r,q}^{(i,j)} \tag{34}$$

where $\mathbf{\Phi}_{r,q}^{(i,j)} = \mathrm{diag}\left\{\frac{\mathbf{a}_{r,q,1}^{(i)}}{\mathbf{a}_{r,q,1}^{(j)}}, \frac{\mathbf{a}_{r,q,2}^{(i)}}{\mathbf{a}_{r,q,2}^{(j)}}, \cdots, \frac{\mathbf{a}_{r,q,K}^{(i)}}{\mathbf{a}_{r,q,K}^{(j)}}\right\}$ with $i,j = 1,2,3,4,5,6$.

Let $\beta_{r,q,k}^{(i,j)}$ represent the kth entry of $\mathbf{\Phi}_{r,q}^{(i,j)}$. And construct $\hat{\mathbf{e}}_{r,q,k} = [1, \beta_{r,q,k}^{(1,2)}, \beta_{r,q,k}^{(1,3)}]^T$ and $\hat{\mathbf{w}}_{r,q,k} = [\beta_{r,q,k}^{(1,4)}, \beta_{r,q,k}^{(1,5)}, \beta_{r,q,k}^{(1,6)}]^T$. Thereafter, the estimates of the normalized Poynting vector at the qth receive EMVS with respect to the kth target can be expressed as

$$\begin{bmatrix} \hat{u}_{r,q,k} \\ \hat{v}_{r,q,k} \\ \hat{w}_{r,q,k} \end{bmatrix} = \frac{\hat{\mathbf{e}}_{r,q,k}}{\| \hat{\mathbf{e}}_{r,q,k} \|} \circ \frac{\hat{\mathbf{w}}_{r,q,k}}{\| \hat{\mathbf{w}}_{r,q,k} \|} \tag{35}$$

Then, the 2D-DOA at the qth receive EMVS with respect to the kth target can be calculated via

$$\begin{cases} \hat{\theta}_{r,q,k} = \arcsin(\sqrt{\hat{v}_{r,q,k}^2 + \hat{u}_{r,q,k}^2}) \\ \hat{\phi}_{r,q,k} = \arctan\left(\frac{\hat{v}_{r,q,k}}{\hat{u}_{r,q,k}}\right) \end{cases} \tag{36}$$

Further, based on the obtained estimates of the 2D-DOA at the qth receive EMVS with respect to the kth target, the corresponding polarization vector can be calculated as follows

$$\hat{\mathbf{g}}_{r,q,k} = \hat{\mathbf{V}}^{+}(\theta_{r,q,k}, \phi_{r,q,k})\hat{\mathbf{a}}_{r,q,k} \tag{37}$$

Thus, the 2D-RPA at the qth receive EMVS with respect to the kth target can be calculated via

$$\begin{cases} \hat{\gamma}_{r,q,k} = \arctan\left(\left|\frac{\hat{\mathbf{g}}_{r,q,k}(1)}{\hat{\mathbf{g}}_{r,q,k}(2)}\right|\right) \\ \hat{\eta}_{r,q,k} = \mathrm{angle}\left(\frac{\hat{\mathbf{g}}_{r,q,k}(1)}{\hat{\mathbf{g}}_{r,q,k}(2)}\right) \end{cases} \tag{38}$$

According to the relationship of the array geometry illustrated in Fig. 1, the position-to-angle related parameter equations for receiver arrays can be established as Eq. (39) at the top of next page.

Subsequently, the coefficient matrices and constant term matrices of Eq. (39) can be obtained by

$$\begin{cases} \mathbf{F}_{r,k} = \begin{bmatrix} \tan\hat{\phi}_{r,1,k} & -1 & 0 \\ \vdots & \vdots & \vdots \\ \tan\hat{\phi}_{r,Q,k} & -1 & 0 \\ 0 & -1 & \tan\hat{\theta}_{r,1,k}\sin\hat{\phi}_{r,1,k} \\ \vdots & \vdots & \vdots \\ 0 & -1 & \tan\hat{\theta}_{r,Q,k}\sin\hat{\phi}_{r,Q,k} \end{bmatrix} \\ \mathbf{G}_{r,k} = \begin{bmatrix} d_r^{(y)} - y_{r,1} - \tan\hat{\phi}_{r,1,k}(d_r^{(x)} - x_{r,1}) \\ \vdots \\ d_r^{(y)} - y_{r,Q} - \tan\hat{\phi}_{r,Q,k}(d_r^{(x)} - x_{r,Q}) \\ d_r^{(y)} - y_{r,1} + \tan\hat{\theta}_{r,1,k}\sin\hat{\phi}_{r,1.k}z_{r,1} \\ \vdots \\ d_r^{(y)} - y_{r,Q} + \tan\hat{\theta}_{r,Q,k}\sin\hat{\phi}_{r,Q,k}z_{r,Q} \end{bmatrix} \end{cases} \tag{40}$$

In a compact matrix form, Eq. (39) can be written, as a whole, in the following

$$\mathbf{F}_{r,k}\mathbf{\Theta}_{r,k} = \mathbf{G}_{r,k} \tag{41}$$

where $\mathbf{\Theta}_{r,k} = \begin{bmatrix} \hat{r}_{r,k}\sin\hat{\theta}_{r,k}\cos\hat{\phi}_{r,k} \\ \hat{r}_{r,k}\sin\hat{\theta}_{r,k}\sin\hat{\phi}_{r,k} \\ \hat{r}_{r,k}\cos\hat{\theta}_{r,k} \end{bmatrix}$.

Utilizing the least squares method, $\hat{\mathbf{\Theta}}_{r,k}$ can be computed by

$$\hat{\mathbf{\Theta}}_{r,k} = (\mathbf{F}_{r,k}^H\mathbf{F}_{r,k})^{-1}\mathbf{F}_{r,k}^H\mathbf{G}_{r,k} \tag{42}$$

Finally, the estimates of the 2D-DOA and RFTR of the kth target corresponding to the reference element can be represented by

$$\begin{cases} \hat{\theta}_{r,k} = \arctan\left(\frac{\sqrt{\hat{\mathbf{\Theta}}_k^2(1,1)+\hat{\mathbf{\Theta}}_k^2(2,1)}}{\hat{\mathbf{\Theta}}_k(3,1)}\right) \\ \hat{\phi}_{r,k} = \arctan\left(\frac{\hat{\mathbf{\Theta}}_k(2,1)}{\hat{\mathbf{\Theta}}_k(1,1)}\right) \\ \hat{r}_{r,k} = \sqrt{\hat{\mathbf{\Theta}}_k^2(1,1) + \hat{\mathbf{\Theta}}_k^2(2,1) + \hat{\mathbf{\Theta}}_k^2(3,1)} \end{cases} \tag{43}$$

Now we have achieved estimation of all the parameters of interest of NF targets for EMVS-MIMO radar. The main steps of the proposed algorithm are summarized in Table I.

$$\begin{cases} \tan\phi_{r,q,k} r_{r,k} \sin\theta_{r,k} \cos\phi_{r,k} - r_{r,k} \sin\theta_{r,k} \sin\phi_{r,k} = d_r^{(y)} - y_{r,k} - \tan\hat{\phi}_{r,q,k}(d_r^{(x)} - x_{r,k}) \\ -r_{r,k} \sin\theta_{r,k} \sin\phi_{r,k} + \tan\hat{\theta}_{r,q,k} \sin\hat{\phi}_{r,q,k} \hat{r}_{r,k} \cos\hat{\theta}_{r,k} = d_r^{(y)} - y_{r,q} + \tan\hat{\theta}_{r,q,k} \sin\hat{\phi}_{r,q,k} z_{r,q} \end{cases} \tag{39}$$

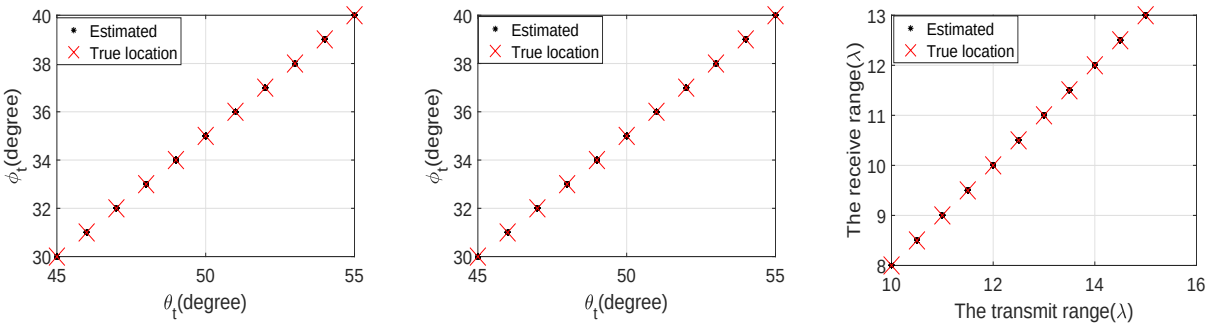

(a) 2D-DOD estimation. (b) 2D-DOA estimation. (c) RFTT and RFTR estimation.

Fig. 2. Scattering diagram of estimated values of the proposed method.

TABLE I
MAIN STEPS OF THE PROPOSED ALGORITHM.

Step	Operation
Step 1	Construct the array covariance matrix $\hat{\mathbf{R}}$, and restructure it into a fourth-order tensor as in Eq. (18).
Step 2	Compress $\mathcal{R}$ into a third-order PARAFAC data model $\tilde{\mathcal{R}}$, and execute PARAFAC decomposition on $\tilde{\mathcal{R}}$ to calculate $\hat{\mathbf{H}}_t$ and $\hat{\mathbf{H}}_r$.
Step 3	Construct a system of equations according to Eq. (31) and obtain $\hat{\mathbf{\Theta}}_{t,k}$ via Eq. (32).
Step 4	Obtain the estimates of 2D-DOD and RFTT via Eq. (33).
Step 5	Formulate $\mathbf{J}_{r,q}$, and further obtain $\mathbf{W}_{r,q}$.
Step 6	Obtain $\mathbf{\Phi}_{r,q}^{(i,j)}$ via Eq. (34), and construct $\hat{\mathbf{e}}_{r,q,k}$ and $\hat{\mathbf{w}}_{r,q,k}$ to obtain $\hat{\theta}_{r,q,k}$ and $\hat{\phi}_{r,q,k}$ according to Eq.(36).
Step 7	Compute $\hat{\mathbf{g}}_{r,q,k}$ via Eq. (37), and then obtain $\hat{\gamma}_{r,q,k}$ and $\hat{\eta}_{r,q,k}$ with Eq. (38).
Step 8	Utilize the LS method to solve the linear equation in Eq.(41), and finally obtain the estimates of 2D-DOA and RFTR via Eq. (43).

V. ALGORITHM ANALYSIS

A. Deterministic Cramer-Rao Bound

In this subsection, the deterministic CRB is developed for the analyzed bistatic MIMO system in which both the transmitter and the receiver are equipped with arbitrary EMVSs.

First, define $\mathbf{\Theta} = [\boldsymbol{\theta}_t^T, \boldsymbol{\theta}_r^T, \mathbf{r}_t^T, \mathbf{r}_r^T, \boldsymbol{\varphi}_t^T, \boldsymbol{\varphi}_r^T]^T$ with $\boldsymbol{\theta}_t = [\theta_{t,1}, \cdots, \theta_{t,K}]^T$, $\boldsymbol{\theta}_r = [\theta_{r,1}, \cdots, \theta_{r,K}]^T$, $\mathbf{r}_t = [r_{t,1}, \cdots, r_{t,K}]^T$, $\mathbf{r}_r = [r_{r,1}, \cdots, r_{r,K}]^T$, $\boldsymbol{\varphi}_t = [\varphi_{t,1}, \cdots, \varphi_{t,K}]^T$ and $\boldsymbol{\varphi}_r = [\varphi_{r,1}, \cdots, \varphi_{r,K}]^T$. Then, the (p,q)th entry of the $6K \times 6K$ CRB matrix for the parameters in $\mathbf{\Theta}$ can be denoted as [34–36]

$$[CRB^{-1}]_{p,q} = \frac{2L}{\sigma_n^2} \mathrm{Re}\left\{ \frac{\partial \mathbf{H}^H}{\partial \mathbf{\Theta}_p} \mathbf{P}_{\mathbf{H}}^{\perp} \frac{\partial \mathbf{H}}{\partial \mathbf{\Theta}_q} \mathbf{R}_U \right\} \tag{44}$$

where $\mathbf{H} = \mathbf{H}_t \odot \mathbf{H}_r$, $\mathbf{P}_{\mathbf{H}}^{\perp} = \mathbf{I}_{6PQ} - \mathbf{H}(\mathbf{H}^H\mathbf{H})^{-1}\mathbf{H}^H$, and $\mathbf{R}_U = \frac{1}{L}\mathbf{U}^H\mathbf{U}$.

Define $\tilde{\mathbf{H}} = [\mathbf{H}_{\theta_t}, \mathbf{H}_{\theta_r}, \mathbf{H}_{r_t}, \mathbf{H}_{r_r}, \mathbf{H}_{\varphi_t}, \mathbf{H}_{\varphi_r}]$ with $\mathbf{H}_{\theta_t} = \left[\frac{\partial \mathbf{h}_1}{\partial \theta_{t,1}}, \cdots, \frac{\partial \mathbf{h}_K}{\partial \theta_{t,K}}\right]$, $\mathbf{H}_{\theta_r} = \left[\frac{\partial \mathbf{h}_1}{\partial \theta_{r,1}}, \cdots, \frac{\partial \mathbf{h}_K}{\partial \theta_{r,K}}\right]$, $\mathbf{H}_{r_t} = \left[\frac{\partial \mathbf{h}_1}{\partial r_{t,1}}, \cdots, \frac{\partial \mathbf{h}_K}{\partial r_{t,K}}\right]$, $\mathbf{H}_{r_r} = \left[\frac{\partial \mathbf{h}_1}{\partial r_{r,1}}, \cdots, \frac{\partial \mathbf{h}_K}{\partial r_{r,K}}\right]$, $\mathbf{H}_{\varphi_t} = \left[\frac{\partial \mathbf{h}_1}{\partial \varphi_{t,1}}, \cdots, \frac{\partial \mathbf{h}_K}{\partial \varphi_{t,K}}\right]$ and $\mathbf{H}_{\varphi_r} = \left[\frac{\partial \mathbf{h}_1}{\partial \varphi_{r,1}}, \cdots, \frac{\partial \mathbf{h}_K}{\partial \varphi_{r,K}}\right]$. After a series of simplifications, the closed-form expression for the CRB can be denoted as

$$CRB = \frac{\sigma^2}{2L}\left[\mathrm{Re}\left\{\left(\tilde{\mathbf{H}}^H \mathbf{\Pi}_{\mathbf{H}}^{\perp} \tilde{\mathbf{H}}\right) \oplus \left(\mathbf{R}_U^T \otimes \mathbf{1}_{6\times 6}\right)\right\}\right]^{-1}. \tag{45}$$

The detailed derivations are provided in the Appendix.

B. Computational Complexity

As it is difficult to find the exact computational complexity of the proposed method, we only make an approximate estimation for the dominant components. The proposed method's computational complexity mainly consists of: (1) PARAFAC decomposition of the covariance matrix with $O\left(PK^2 + 6QK^2 + 6PQK^2\right)$ flops, and (2) computation of $\mathbf{\Phi}_{r,q}^{(i,j)}$ $(q = 1, \cdots Q)$ with $O\left(5QK^2\right)$ flops. Therefore, the presented method has a computational complexity of $O\left(PK^2 + 11QK^2 + 6PQK^2\right)$.

C. The maximum number of identifiable targets

Suppose that the maximum number of identifiable targets is K. The value of K is related to the uniqueness condition of PARAFAC decomposition, which is dependent on the Kruskal's theorem. It can be observed that $\max(k_{\mathbf{H}_t}) = P$, $\max\{k_{\mathbf{H}_r}\} = 6Q$ and $\max\{k_{\tilde{\mathbf{H}}^*}\} = 6PQ$, so the value of K can be calculated as

$$K = \frac{P + 6Q + 6PQ - 3}{2}. \tag{46}$$

Besides, the value of K relies also on the rotation invariant relationship in Eq. (34), which satisfies

$$K \leqslant 6Q - 1. \tag{47}$$

Therefore, based on Eq. (46) and Eq. (47), the value of K is

$$K = 6Q - 1. \tag{48}$$

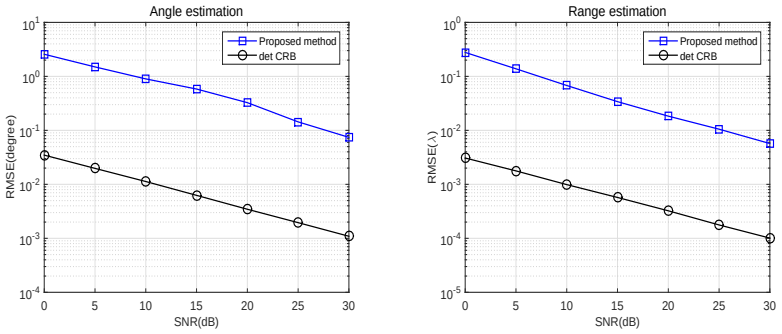

(a) (b)

Fig. 3. RMSE results versus SNR.

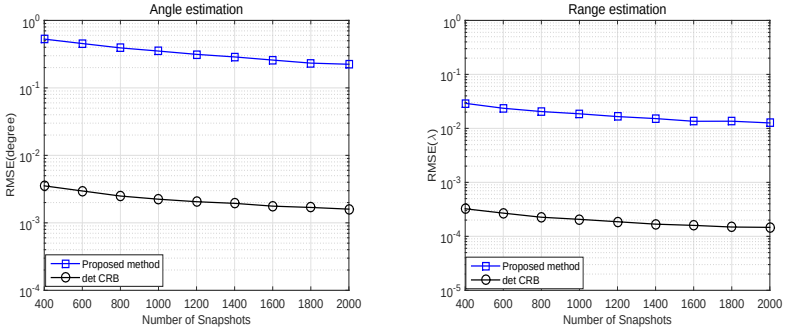

(a) (b)

Fig. 4. RMSE results versus the number of snapshots.

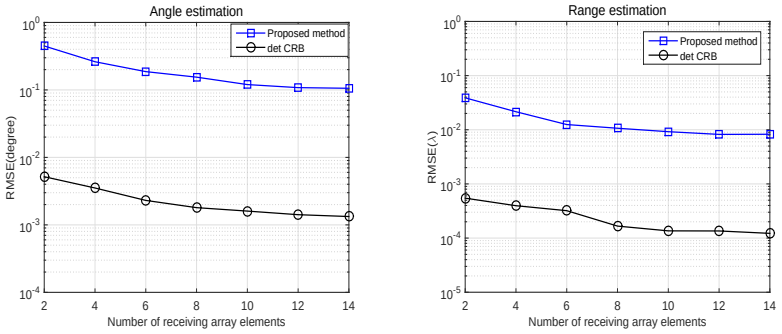

(a) (b)

Fig. 5. RMSE results versus the number of receive array elements.

TABLE II
POLARIZATION PARAMETER ESTIMATION.

	$\gamma_{r,1,1}(\circ)$ 31	$\gamma_{r,2,1}(\circ)$ 32	$\gamma_{r,3,1}(\circ)$ 33	$\gamma_{r,4,1}(\circ)$ 34	$\gamma_{r,5,1}(\circ)$ 35	$\gamma_{r,1,2}(\circ)$ 41	$\gamma_{r,2,2}(\circ)$ 42	$\gamma_{r,3,2}(\circ)$ 43	$\gamma_{r,4,2}(\circ)$ 44	$\gamma_{r,5,2}(\circ)$ 45
Estimated	30.9974	31.9997	32.9987	33.9986	34.9996	41.0044	41.9977	43.0001	43.9996	44.9989
RMSE	0.0011	0.0009	0.0015	0.0011	0.0008	0.0016	0.0011	0.0018	0.0014	0.0009
	$\eta_{r,1,1}(\circ)$ 11	$\eta_{r,2,1}(\circ)$ 12	$\eta_{r,3,1}(\circ)$ 13	$\eta_{r,4,1}(\circ)$ 14	$\eta_{r,5,1}(\circ)$ 15	$\eta_{r,1,2}(\circ)$ 21	$\eta_{r,2,2}(\circ)$ 22	$\eta_{r,3,2}(\circ)$ 23	$\eta_{r,4,2}(\circ)$ 24	$\eta_{r,5,2}(\circ)$ 25
Estimated	11.0060	11.9984	12.9980	14.0031	14.9996	20.9945	21.9998	23.0008	23.9958	24.9990
RMSE	0.0042	0.0042	0.0042	0.0038	0.0040	0.0037	0.0042	0.0044	0.0042	0.0039

VI. Simulation Results

Simulations are conducted to assess the effectiveness of the proposed algorithms in this section. Unless otherwise specified, assume that the bistatic MIMO radar system is furnished with five EMVS at both the transmitter and the receiver with $(x_{t,p}, y_{t,p}, z_{t,p})$ = (-2.5λ,-2.5λ,-2.5λ), (1λ,0.5λ,2λ), (1.5λ,-1λ,-1λ), (-1λ,0.5λ,0.5λ), (2.5λ,2.5λ,2.5λ) and $(x_{r,q}, y_{r,q}, z_{r,q})$ = (-5λ,-5λ,-5λ), (2λ,-2λ,2λ), (3λ,-3λ,3λ), (-5λ,4.5λ,5λ), (-4λ,-2.5λ,-2.5λ), respectively. There are two NF uncorrelated targets with parameters $\theta_t = (60^\circ, 30^\circ)$, $\varphi_t = (30^\circ, 60^\circ)$, $r_t = (10\lambda, 12\lambda)$, $\theta_r = (50^\circ, 20^\circ)$, $\varphi_r = (20^\circ, 50^\circ)$, $r_r = (8\lambda, 15\lambda)$, $(\gamma_{r,1,1}, \gamma_{r,2,1}, \cdots, \gamma_{r,5,2}) = (31^\circ, 32^\circ, 33^\circ, 34^\circ, 35^\circ, 41^\circ, 42^\circ, 43^\circ, 44^\circ, 45^\circ)$ and $(\eta_{r,1,1}, \eta_{r,2,1}, \cdots, \eta_{r,5,2}) = (11^\circ, 12^\circ, 13^\circ, 14^\circ, 15^\circ, 21^\circ, 22^\circ, 23^\circ, 24^\circ, 25^\circ)$. and All simulations are based on 500 statistically independent Monte-Carlo trials. In addition, the root mean square error (RMSE) is employed to evaluate the performance of the proposed algorithm, defined as

$$\text{RMSE} = \sqrt{\frac{1}{500K}\sum_{k=1}^{K}\sum_{i=1}^{500}\left(\hat{\vartheta}_{i.k} - \vartheta_k\right)^2} \tag{49}$$

where $\hat{\vartheta}_{i.k}$ accounts for the estimate of the parameters $\theta_{t,k}$, $\varphi_{t,k}$, $r_{t,k}$, $\theta_{r,k}$, $\varphi_{r,k}$ and $r_{r,k}$, at the ith trial, while ϑ_k denotes the true value.

Simulation 1: In the first simulation, the bistatic MIMO radar system is equipped with two EMVS elements (Q=2) at both the transmitter and the receiver with $(x_{t,m}, y_{t,m}, z_{t,m}) = (-2.5\lambda, -2.5\lambda, -2.5\lambda)$, (1$\lambda$,0.5$\lambda$,2$\lambda$) and $(x_{r,n}, y_{r,n}, z_{r,n}) = (-5\lambda, -5\lambda, -5\lambda)$, (2$\lambda$, - 2$\lambda$,2$\lambda$). In order to verify the maximum number of identifiable targets by the proposed method, the scatting diagram results are shown in Fig. 2 for the 6-D parameters (2D-DOD, 2D-DOA, RFTT and RFTR) under the signal-to-noise ratio (SNR) of 50dB, where the number of snapshots is 50000. It can be clearly seen that when the bistatic MIMO radar system is equipped with two EMVS elements at both the transmitter and the receiver, the proposed method can accurately estimate the parameters of 11 targets, which are automatically paired.

Simulation 2: In the second simulation, the RMSE is adopted to verify the performance of the proposed method, and the deterministic CRB is given as a performance benchmark. Fig. 3 presents the estimation results for angle, range and polarization parameters with respect to SNR, and the number of snapshots is 1000. As can be seen, the RMSEs decrease as SNR increases, clearly showing that the proposed method effectively locates the 3-D NF sources and properly identifies the polarization parameters. Additionally, note that the RMSEs for the angle and the range parameters do not approach the deterministic CRB effectively, mainly because the presented method only exploits the information inside the electromagnetic vector without taking advantage of the array aperture.

Simulation 3: In the third simulation, the estimation results of polarization parameters are presented in Table II, where the number of snapshot is set to 2000, the SNR is fixed at 25dB, and the other settings are the same as **Simulation 2**. Obviously, the proposed method can accurately estimate all the polarization parameters.

Simulation 4: In this simulation, the RMSE results for angle and range with the number of snapshots varying from 400 to 2000 are presented in Fig. 4, where the SNR is fixed at 20dB, and the other settings are the same as **Simulation 2**. It can be seen that the RMSE results decrease as the number of snapshots increases, which improves the time diversity gain. In addition, the explanation for the clear gap between the RMSEs of the angle and range parameters and the associated deterministic CRBs is the same as stated in the second simulation.

Simulation 5: To verify the performance of the proposed method with respect to the number of receive antennas, the RMSE results for angle and range are provided in Fig. 5, with SNR=20dB, $L = 1000$, and $P = 5$. For a fixed number of transmit antennas, the RMSEs of all parameters decrease as the number of receive antennas becomes large, given the increased degrees of freedom provided for exploiting the space diversity gain in a MIMO system.

Simulation 6: In this simulation, in order to demonstrate the spatial resolution of the proposed method, we examine the probability of successful detection (PSD) with two targets. Define PSD $= T/500$, where T records the trial number that the absolute errors of estimated angles/range are under $1^\circ/1\lambda$. The suffix '-d' in the legend denotes the result computed by taking the mean value of four direction angles (2D-DOA and 2D-DOD), and the suffix '-r' denotes the result calculated by taking the mean value on two ranges (RFTT and RFTR). Fig. 6 shows the PSD performance, where the two targets' parameters $(\theta_t, \theta_r, \phi_t, \phi_r, r_t, r_r)$ are $(45^\circ, 50^\circ, 25^\circ, 20^\circ, 3\lambda, 8\lambda)$ and $(46^\circ, 51^\circ, 26^\circ, 21^\circ, 4\lambda, 9\lambda)$, and the other simulation parameters are the same as in **Simulation 2**. It can be clearly observed from Fig. 6 that the proposed method offers 100% PSD for angles and ranges with the SNR at 0dB and 20dB, respectively, with angle and range intervals being 1° and 1λ.

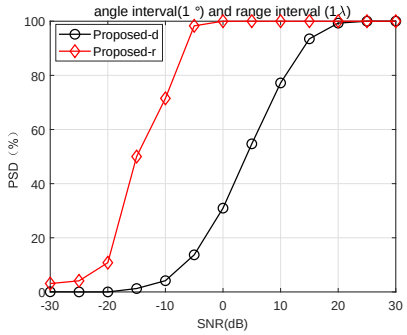

Fig. 6. Illustration of PSD versus SNR.

VII. Conclusion

In this paper, the estimation of multi-parameters for 3-D NF sources has been studied in a bistatic MIMO radar system furnished with arbitrary EMVSs. A covariance-based trilinear decomposition method is proposed to find the multiple

parameters, by fully making use of the tensor structure of the covariance matrix. In addition, the obtained 2D-DOD, 2D-DOA, RFTT, RFTR, and 2D-RPA parameters can be automatically paired and their estimation results have a closed-form expression. Moreover, the CRB has also been deduced as a performance benchmark. As shown by the provided numerical simulation results, the presented method has attained a satisfactory performance, although further improvement is needed in the future given the clear gap between its performance and the derived CRB.

APPENDIX

A. CRB derivation

Firstly, let $\mathbf{Y}=\left[\mathbf{y}^T(1),\mathbf{y}^T(2),\cdots,\mathbf{y}^T(L)\right]^T$. According to Eq.(6), the mean $\boldsymbol{\mu}$ of $\mathbf{Y}$ can be expressed as

$$\boldsymbol{\mu}=\begin{bmatrix}\mathbf{Hu}(1)\\ \mathbf{Hu}(2)\\ \vdots\\ \mathbf{Hu}(L)\end{bmatrix}=\mathbf{E\Gamma} \tag{50}$$

where $\mathbf{H}=\mathbf{H}_t\odot\mathbf{H}_r$, $\mathbf{E}=\mathbf{H}\otimes\mathbf{I}_L$, and $\mathbf{\Gamma}=\left[\mathbf{u}^T(1),\mathbf{u}^T(2),\cdots,\mathbf{u}^T(L)\right]^T$.

Then, we define two unknown parameter vectors $\boldsymbol{\alpha}=\left[\boldsymbol{\theta}_t^T,\boldsymbol{\theta}_r^T,\mathbf{r}_t^T,\mathbf{r}_r^T,\boldsymbol{\varphi}_t^T,\boldsymbol{\varphi}_r^T\right]$ with $\boldsymbol{\theta}_t=[\theta_{t1},\theta_{t2},\cdots,\theta_{tK}]^T$, $\boldsymbol{\theta}_r=[\theta_{r1},\theta_{r2},\cdots,\theta_{rK}]^T$, $\mathbf{r}_t=[r_{t1},r_{t2},\cdots,r_{tK}]^T$, $\mathbf{r}_r=[r_{r1},r_{r2},\cdots,r_{rK}]^T$, $\boldsymbol{\varphi}_t=[\varphi_{t1},\varphi_{t2},\cdots,\varphi_{tK}]^T$ and $\boldsymbol{\varphi}_r=[\varphi_{r1},\varphi_{r2},\cdots,\varphi_{rK}]^T$, along with $\boldsymbol{\beta}=\left[\mathrm{Re}\left\{\mathbf{\Upsilon}^T\right\},\mathrm{Im}\left\{\mathbf{\Upsilon}^T\right\}\right]^T$. Combining these two together, a new parameter vector is then constructed as $\boldsymbol{\xi}=\left[\boldsymbol{\alpha}^T,\boldsymbol{\beta}\right]^T$. As stated in [25], the CRB matrix for $\boldsymbol{\xi}$ is denoted as

$$CRB=\frac{\sigma^2}{2}\left[\mathrm{Re}\left\{\mathbf{\Omega}^H\mathbf{\Omega}\right\}\right]^{-1} \tag{51}$$

where $\mathbf{\Omega}=\left[\frac{\partial\boldsymbol{\mu}}{\partial\boldsymbol{\alpha}^T},\frac{\partial\boldsymbol{\mu}}{\partial\boldsymbol{\beta}^T}\right]$.

To simplify Eq. (44), we derive the related items as follows

$$\frac{\partial\boldsymbol{\mu}}{\partial\boldsymbol{\beta}^T}=[\mathbf{E},j\mathbf{E}] \tag{52}$$

$$\begin{aligned}\frac{\partial\boldsymbol{\mu}}{\partial\boldsymbol{\theta}_t^T}&=\begin{bmatrix}\left(\frac{\partial\mathbf{h}_1}{\partial\theta_{t1}}\right)u_1(1) & \cdots & \left(\frac{\partial\mathbf{h}_K}{\partial\theta_{tK}}\right)u_K(1)\\ \vdots & \ddots & \vdots\\ \left(\frac{\partial\mathbf{h}_1}{\partial\theta_{t1}}\right)u_1(L) & \cdots & \left(\frac{\partial\mathbf{h}_K}{\partial\theta_{tK}}\right)u_K(L)\end{bmatrix}\\ &=\mathbf{H}_{\theta_t}\odot\mathbf{U}\end{aligned} \tag{53}$$

where $\mathbf{h}_k$ is the k-th column of $\mathbf{H}$, and $\mathbf{H}_{\theta_t}=\left[\frac{\partial\mathbf{h}_1}{\partial\theta_{t1}},\cdots,\frac{\partial\mathbf{h}_K}{\partial\theta_{tK}}\right]$. Thus, we can obtain

$$\frac{\partial\boldsymbol{\mu}}{\partial\boldsymbol{\alpha}^T}=[\mathbf{H}_{\theta_t}\odot\mathbf{U},\mathbf{H}_{\theta_r}\odot\mathbf{U},\cdots,\mathbf{H}_{\varphi_r}\odot\mathbf{U}]=\mathbf{\Delta}. \tag{54}$$

Furthermore, we have

$$\mathbf{J}=\mathrm{Re}\left\{\mathbf{\Omega}^H\mathbf{\Omega}\right\}=\mathrm{Re}\left\{\begin{bmatrix}\mathbf{\Delta}^H\\ \mathbf{O}^H\\ -j\mathbf{O}^H\end{bmatrix}[\mathbf{\Delta},\mathbf{O},j\mathbf{O}]\right\} \tag{55}$$

Since we are only interested in CRB for angle and range estimation, diagonalization is exploited to extract these corresponding terms from $\mathbf{J}$.

Define

$$\mathbf{V}_\Delta=\left(\mathbf{O}^H\mathbf{O}\right)^{-1}\mathbf{O}^H\mathbf{\Delta} \tag{56}$$

As $\mathbf{O}^H\mathbf{O}$ is nonsingular, $\mathbf{V}_\nabla^{-1}$ is valid, and we define

$$\mathbf{P}=\begin{bmatrix}\mathbf{I}_{2K} & \mathbf{0} & \mathbf{0}\\ -\mathrm{Re}\{\mathbf{V}_\Delta\} & \mathbf{I} & \mathbf{0}\\ -\mathrm{Im}\{\mathbf{V}_\Delta\} & \mathbf{0} & \mathbf{I}\end{bmatrix} \tag{57}$$

Then, we can find

$$[\mathbf{\Delta},\mathbf{O},j\mathbf{O}]\,\mathbf{P}=[(\mathbf{\Delta}-\mathbf{OV}_\Delta),\mathbf{O},j\mathbf{O}] \tag{58}$$

Let $\mathbf{\Pi}_{\mathbf{H}}^{\perp}$ represent the orthogonal projection of $\mathbf{H}^H$ onto the null space, i.e.,

$$\mathbf{\Pi}_{\mathbf{O}}^{\perp}=\mathbf{I}_{6PQL}-\mathbf{O}\left(\mathbf{O}^H\mathbf{O}\right)^{-1}\mathbf{O}^H \tag{59}$$

Thus, we have $\mathbf{O}^H\mathbf{\Pi}_{\mathbf{O}}^{\perp}=0$, and further obtain

$$\begin{aligned}\mathbf{P}^H\mathbf{JP}&=\mathrm{Re}\left\{\begin{bmatrix}\mathbf{\Delta}^H\mathbf{\Pi}_{\mathbf{O}}^{\perp}\\ \mathbf{O}^H\\ -j\mathbf{O}^H\end{bmatrix}\left[\mathbf{\Pi}_{\mathbf{O}}^{\perp}\mathbf{\Delta},\mathbf{O},j\mathbf{O}\right]\right\}\\ &=\mathrm{Re}\left\{\begin{bmatrix}\mathbf{\nabla} & \mathbf{0} & \mathbf{0}\\ \mathbf{0} & \mathbf{O}^H\mathbf{O} & j\mathbf{O}^H\mathbf{O}\\ \mathbf{0} & -j\mathbf{O}^H\mathbf{O} & \mathbf{O}^H\mathbf{O}\end{bmatrix}\right\}\end{aligned} \tag{60}$$

where $\mathbf{\nabla}=\mathbf{\Delta}^H\mathbf{\Pi}_E^{\perp}\mathbf{\Delta}$.

According to the property of a partitioned diagonal matrix, we have

$$\begin{aligned}\mathbf{J}^{-1}&=\mathbf{P}\left(\mathbf{P}^H\mathbf{JP}\right)^{-1}\mathbf{P}^T\\ &=\begin{bmatrix}\mathbf{I} & \mathbf{0}\\ \times & \mathbf{I}\end{bmatrix}\begin{bmatrix}\mathrm{Re}\{\mathbf{\nabla}\} & \mathbf{0}\\ \mathbf{0} & \times\end{bmatrix}^{-1}\begin{bmatrix}\mathbf{I} & \times\\ \mathbf{0} & \mathbf{I}\end{bmatrix}\\ &=\begin{bmatrix}\mathrm{Re}\{\mathbf{\nabla}\} & \mathbf{0}\\ \mathbf{0} & \times\end{bmatrix}^{-1}\end{aligned} \tag{61}$$

where $\times$ denotes the part not needed in the derivation. Substituting Eq.(57) and Eq.(51) into Eq.(47), and eliminating all the unaffected parts, the CRBs for angle and range estimation can be obtained as

$$CRB=\frac{\sigma^2}{2}[\mathrm{Re}\{\mathbf{\nabla}\}]^{-1} \tag{62}$$

Since $\mathbf{O}=\mathbf{H}\otimes\mathbf{I}_L$, we have $\mathbf{\Pi}_{\mathbf{O}}^{\perp}=\mathbf{\Pi}_{\mathbf{H}}^{\perp}\otimes\mathbf{I}_L$.

In addition,$\mathbf{\Delta}$ can be rewritten as

$$\mathbf{\Delta}=[\mathbf{o}_1\otimes\mathbf{u}_1(\cdot),\cdots,\mathbf{u}_{K+1}\otimes\mathbf{u}_1(\cdot),\cdots,\mathbf{o}_{6K}\otimes\mathbf{u}_K(\cdot)] \tag{63}$$

where $\mathbf{o}_m$ represents the m-th column of the matrix $\tilde{\mathbf{H}}=[\mathbf{H}_{\theta_t},\mathbf{H}_{\theta_r},\cdots,\mathbf{H}_{\boldsymbol{\varphi}_r}]$, and $\mathbf{u}_k(\cdot)$ is the k-th column of $\mathbf{U}$.

Since $(\mathbf{E}\otimes\mathbf{F})(\mathbf{G}\otimes\mathbf{Q})=(\mathbf{EG})\otimes(\mathbf{FQ})$, we can obtain

$$\mathbf{\Pi}_{\mathbf{O}}^{\perp}\mathbf{\Delta}=\left[\mathbf{\Pi}_{\mathbf{H}}^{\perp}\mathbf{o}_1\otimes\mathbf{u}_1(\cdot),\cdots,\mathbf{\Pi}_{\mathbf{H}}^{\perp}\mathbf{o}_{6K}\otimes\mathbf{u}_K(\cdot)\right] \tag{64}$$

Therefore,$\boldsymbol{\nabla}$ can be denoted as

$$\begin{aligned}\boldsymbol{\nabla} &= \begin{bmatrix} \mathbf{o}_1^H \otimes \mathbf{u}_1^H(\cdot) \\ \vdots \\ \mathbf{o}_{6K}^H \otimes \mathbf{u}_K^H(\cdot) \end{bmatrix} \boldsymbol{\Pi}_{\mathbf{O}}^{\perp} \boldsymbol{\Delta} \\ &= L \cdot \begin{bmatrix} \mathbf{o}_1^H \boldsymbol{\Pi}_{\tilde{\mathbf{H}}}^{\perp} \mathbf{o}_1 \mathbf{R}_{1,1} & \cdots & \mathbf{o}_1^H \boldsymbol{\Pi}_{\tilde{\mathbf{H}}}^{\perp} \mathbf{o}_{6K} \mathbf{R}_{1,K} \\ \vdots & \ddots & \vdots \\ \mathbf{o}_{6K}^H \boldsymbol{\Pi}_{\tilde{\mathbf{H}}}^{\perp} \mathbf{o}_1 \mathbf{R}_{1,1} & \cdots & \mathbf{o}_{6K}^H \boldsymbol{\Pi}_{\tilde{\mathbf{H}}}^{\perp} \mathbf{o}_{6K} \mathbf{R}_{K,K} \end{bmatrix} \\ &= L \cdot \left(\tilde{\mathbf{H}}^H \boldsymbol{\Pi}_{\tilde{\mathbf{H}}}^{\perp} \tilde{\mathbf{H}} \right) \oplus \left(\mathbf{R}_u^T \otimes \mathbf{1}_{6\times 6} \right) \end{aligned} \tag{65}$$

where $\mathbf{R}_{m,n}$ represents the (m,n)-th entry of $\mathbf{R}_s = \frac{1}{L}\mathbf{U}^H\mathbf{U}$. At last, we get

$$CRB = \frac{\sigma^2}{2L} \left[\mathrm{Re} \left\{ \left(\tilde{\mathbf{H}}^H \boldsymbol{\Pi}_{\tilde{\mathbf{H}}}^{\perp} \tilde{\mathbf{H}} \right) \oplus \left(\mathbf{R}_u^T \otimes \mathbf{1}_{6\times 6} \right) \right\} \right]^{-1} \tag{66}$$

REFERENCES

[1] J. Shi, F. Wen, and T. Liu, "Nested MIMO radar: Coarrays, tensor modeling, and angle estimation," *IEEE Transactions on Aerospace and Electronic Systems*, vol. 57, no. 1, pp. 573–585, 2021.

[2] S. Luo, Y. Wang, J. Li, C. Tellambura, and J. J. P. C. Rodrigues, "Coarray tensor-based angle estimation for bistatic MIMO radar with a dilated moving receive array," *IEEE Transactions on Aerospace and Electronic Systems*, pp. 1–13, 2023.

[3] H. Ma, H. Tao, J. Su, and B. Liao, "DOD/DOA and polarization estimation in MIMO systems with spatially spread dipole quints," *IEEE Communications Letters*, vol. 24, no. 1, pp. 99–102, 2020.

[4] J. Du, W. Yu, L. Jin, X. Li, and D. B. D. Costa, "Tensor-based angle estimation for bistatic MIMO radar systems with multi-slot gain-phase error," *IEEE Transactions on Aerospace and Electronic Systems*, pp. 1–17, 2023.

[5] X. Lai, X. Zhang, W. Zheng, and P. Ma, "Spatially smoothed tensor-based method for bistatic co-prime MIMO radar with hole-free sum-difference co-array," *IEEE Transactions on Vehicular Technology*, vol. 71, no. 4, pp. 3889–3899, 2022.

[6] X. Zhang, Z. Zheng, W.-Q. Wang, and H. C. So, "Joint DOD and DOA estimation of coherent targets for coprime MIMO radar," *IEEE Transactions on Signal Processing*, vol. 71, pp. 1408–1420, 2023.

[7] H. Zhang, D. Xu, and N. Wang, "Explicit joint resolution limit for range and direction of arrival estimation in MIMO radar," *IEEE Transactions on Aerospace and Electronic Systems*, pp. 1–10, 2023.

[8] P. Gong, W. Q. Wang, and X. Wan, "Adaptive weight matrix design and parameter estimation via sparse modeling for MIMO radar," *Signal Processing*, vol. 139, pp. 1–11, 2017.

[9] X. Zhang, L. Xu, L. Xu, and D. Xu, "Direction of departure (DOD) and direction of arrival (DOA) estimation in MIMO radar with reduced-dimension MUSIC," *IEEE Communications Letters*, vol. 14, no. 12, pp. 1161–1163, 2010.

[10] D. Chen, B. Chen, and G. Qin, "Angle estimation using ESPRIT in MIMO radar," *Electronics Letters*, vol. 44, pp. 770–771, 2008.

[11] D. Nion and N. D. Sidiropoulos, "Tensor algebra and multidimensional harmonic retrieval in signal processing for MIMO radar," *IEEE Transactions on Signal Processing*, vol. 58, no. 11, pp. 5693–5705, 2010.

[12] T.-Q. Xia, "Joint diagonalization based 2D-DOD and 2D-DOA estimation for bistatic MIMO radar," *Signal Processing*, vol. 116, pp. 7–12, 2015.

[13] X. Wu, Y. Liu, and X. Yang, "Efficient gridless angle estimation for bistatic MIMO radar with planar arrays," *IEEE Transactions on Vehicular Technology*, vol. 71, no. 5, pp. 5599–5603, 2022.

[14] H. Ma, H. Tao, J. Xie, and X. Cheng, "Parameters estimation of 3-D near-field sources with arbitrarily spaced electromagnetic vector-sensors," *IEEE Communications Letters*, vol. 26, no. 11, pp. 2764–2768, 2022.

[15] A. Nehorai and E. Paldi, "Vector-sensor array processing for electromagnetic source localization," *IEEE Transactions on Signal Processing*, vol. 42, no. 2, pp. 376–398, 1994.

[16] X. Wang, Y. Guo, F. Wen, J. He, and T.-K. Truong, "EMVS-MIMO radar with sparse Rx geometry: Tensor modeling and 2-D direction finding," *IEEE Transactions on Aerospace and Electronic Systems*, vol. 59, no. 6, pp. 8062–8075, 2023.

[17] S. Chintagunta and P. Ponnusamy, "2D-DOD and 2D-DOA estimation using the electromagnetic vector sensors," *Signal Processing*, vol. 147, 2018.

[18] F. Wen, J. Shi, and Z. Zhang, "Joint 2D-DOD, 2D-DOA, and polarization angles estimation for bistatic EMVS-MIMO radar via PARAFAC analysis," *IEEE Transactions on Vehicular Technology*, vol. 69, no. 2, pp. 1626–1638, 2020.

[19] F. Wen, J. Shi, J. He, and T.-K. Truong, "2D-DOD and 2D-DOA estimation using sparse l-shaped EMVS-MIMO radar," *IEEE Transactions on Aerospace and Electronic Systems*, vol. 59, no. 2, pp. 2077–2084, 2023.

[20] F. Wen, J. Shi, and Z. Zhang, "Closed-form estimation algorithm for EMVS-MIMO radar with arbitrary sensor geometry," *Signal Processing*, vol. 186, no. 8, p. 108117, 2021.

[21] E. Zhou, H. Jiang, and H. Qi, "4-D parameter estimation in bistatic MIMO radar for near-field target localization," in *2015 IEEE International Wireless Symposium (IWS 2015)*, 2015, pp. 1–4.

[22] A. M. Molaei, P. del Hougne, V. Fusco, and O. Yurduseven, "Efficient joint estimation of DOA, range and reflectivity in near-field by using mixed-order statistics and a symmetric MIMO array," *IEEE Transactions on Vehicular Technology*, vol. 71, no. 3, pp. 2824–2842, 2022.

[23] P. Singh, Y. Wang, and P. Charg, "Bistatic MIMO radar for near field source localisation using PARAFAC," *Electronics Letters*, vol. 52, no. 12, pp. 1060–1061, 2016.

[24] I. Podkurkov, L. Hamidullina, E. Traikov, M. Haardt, and A. Nadeev, "Tensor-based near-field localization in bistatic MIMO radar systems," in *WSA 2018; 22nd International ITG Workshop on Smart Antennas*, 2018, pp. 1–8.

[25] L. Khamidullina, I. Podkurkov, and M. Haardt, "Conditional and unconditional cramer-rao bounds for near-field localization in bistatic MIMO radar systems," *IEEE Transactions on Signal Processing*, vol. 69, pp. 3220–3234, 2021.

[26] H. Chen, W. Wang, W. Liu, Y. Tian, and G. Wang, "An exact near-field model based localization for bistatic MIMO radar with COLD arrays," *IEEE Transactions on Vehicular Technology*, vol. 72, no. 12, pp. 16 021–16 030, 2023.

[27] M. Haardt, F. Roemer, and G. Del Galdo, "Higher-order svd-based subspace estimation to improve the parameter estimation accuracy in multidimensional harmonic retrieval problems," *IEEE Transactions on Signal Processing*, vol. 56, no. 7, pp. 3198–3213, 2008.

[28] H. Zheng, C. Zhou, Z. Shi, Y. Gu, and Y. D. Zhang, "Coarray tensor direction-of-arrival estimation," *IEEE Transactions on Signal Processing*, vol. 71, pp. 1128–1142, 2023.

[29] C. Gu, J. He, H. Li, and X. Zhu, "Target localization using MIMO electromagnetic vector array systems," *Signal Processing*, vol. 93, no. 7, pp. 2103–2107, 2013.

[30] T. Shu, J. He, F. Wen, and T.-K. Truong, "Incompletely polarized MIMO radar for target direction estimation," *IEEE Transactions on Radar Systems*, vol. 1, pp. 532–541, 2023.

[31] J.-J. Xiao and A. Nehorai, "Optimal polarized beampattern synthesis using a vector antenna array," *IEEE Transactions on Signal Processing*, vol. 57, no. 2, pp. 576–587, 2009.

[32] ——, "Joint transmitter and receiver polarization optimization for scattering estimation in clutter," *IEEE Transactions on Signal Processing*, vol. 57, no. 10, pp. 4142–4147, 2009.

[33] X. Liu and N. Sidiropoulos, "Cramer-rao lower bounds for low-rank decomposition of multidimensional arrays," *IEEE Transactions on Signal Processing*, vol. 49, no. 9, pp. 2074–2086, 2001.

[34] J. He, M. N. S. Swamy, and M. O. Ahmad, "Efficient application of music algorithm under the coexistence of far-field and near-field sources," *IEEE Transactions on Signal Processing*, vol. 60, no. 4, pp. 2066–2070, 2012.

[35] H. Chen, W. Wang, and W. Liu, "Joint DOA, range, and polarization estimation for rectilinear sources with a COLD array," *IEEE Wireless Communications Letters*, vol. 8, no. 5, pp. 1398–1401, 2019.

[36] J. He, T. Shu, L. Li, and T.-K. Truong, "Mixed near-field and far-field localization and array calibration with partly calibrated arrays," *IEEE Transactions on Signal Processing*, vol. 70, pp. 2105–2118, 2022.